Effects of 3*d* and 4*d* transition metal substitutional impurities on the electronic properties of CrO_2

M. E. Williams,[1] H. Sims,[2,3] D. Mazumdar,[2,3] and W. H. Butler[2,3]

[1]*Department of Mathematics & Computer Science, University of Maryland Eastern Shore, Princess Anne, MD 21853, USA*

[2]*Center for Materials for Information Technology, University of Alabama, Tuscaloosa, AL 35401, USA*

[3]*Department of Physics, University of Alabama, University of Alabama, Tuscaloosa, AL 35401, USA*

(Received 21 July 2011; revised manuscript received 9 July 2012; published 17 December 2012)

We present first-principles-based density functional theory calculations of the electronic and magnetic structure of CrO_2 with 3*d* and 4*d* substitutional impurities. We find that the half-metallicity of CrO_2 remains intact for the ground state of all of the calculated substitutions. We also observe two periodic trends as a function of the number of valence electrons: if the substituted atom has six or fewer valence electrons, the number of down spin electrons associated with the impurity ion is zero, resulting in ferromagnetic alignment of the impurity magnetic moment with the magnetization of the CrO_2 host. For substituent atoms with eight to ten valence electrons (with the exception of Ni), the number of down-spin electrons contributed by the impurity ion remains fixed at three as the number contributed to the majority increases from one to three resulting in antiferromagnetic alignment between impurity moment and host magnetization. In impurities with seven valence electrons, the zero down-spin and threse down-spin configurations are very close in energy. At 11 valence electrons, the energy is minimized when the substituent ion contributes five down-spin electrons. The moments on the 4*d* impurities, particularly Nb and Mo, tend to be delocalized compared with those of the 3*d*s.

DOI: 10.1103/PhysRevB.86.235124 PACS number(s): 31.15.A−, 75.47.Lx, 85.75.−d

I. INTRODUCTION

Rutile structure binary transition metal oxides (general formula XO_2) comprise a very large family that covers much of the periodic table. Known stoichiometric rutile (or distorted rutile) XO_2 compounds span the range from ions with nominal d^0 configuration (X = Ti) to d^1 (X = V, Nb, Ta) to d^2 (X = Cr, Mo, W) to d^3 (X = Mn, Tc, Re) d^4 (X = Ru, Os), to d^5 (X = Rh, Ir) to d^6 (X = Pt) to d^{10} (X = Ge, Sn, Pb).[1] The rutile-structure oxides show extremely diverse electronic properties. In the 3*d* series, d^0 TiO_2 is a nonmagnetic insulator, whereas d^1 vanadium oxide (VO_2) is a strongly correlated oxide showing a metal-semiconductor transition concurrent with a rutile-monoclinic structural transition at ∼340 K.[2] Adding a single electron to VO_2 (i.e., d^2 CrO_2) reduces correlation effects and makes CrO_2 a ferromagnetic (FM) half-metal with a gap in the minority spin channel.[3] As we progress to d^3 MnO_2, the system stabilizes in an antiferromagnetic (AFM) insulating state. However, in the 4*d* (Mo, Tc, Ru, and Rh) and 5*d* (Ta, W, Re, Os Ir, Pt) XO_2 oxides the correlated/semicorrelated behavior is almost lost, and these oxides tend be nonmagnetic metals with a distorted structure.[4] The only exception to this trend is d^1 NbO_2, which is isoelectronic to VO_2, and exhibits a metal-insulator transition, again like VO_2.

Insight into the electronic properties can also be obtained through doping studies. In a previous work we investigated the case of Ru doping into half-metallic CrO_2.[5] We found that Ru formed localized states in the minority channel gap but left the half-metallic feature of the electronic structure intact for low concentrations. In another study, we investigated the electronic and magnetic properties of Cr-doped Vanadium oxide $V_{1-x}Cr_xO_2$[6] and found that the doped rutile-phase material remained FM and half-metallic even for high concentrations. These intriguing results suggest the need for a systematic study of the doping behavior of CrO_2. The present work provides a first step in this direction, which we hope will establish a basis for future experiments and theoretical insights.

We seek to answer the question of what happens when other *d* atoms are substituted into the half-metal CrO_2. We speculate that almost all transition metal ions will substitute for Cr at least to some extent. Here we investigate systematically the effect of adding impurities in CrO_2 by substituting transition metal atoms from the 3*d* and 4*d* series for a Cr atom. In doing so, we explore the behavior of the additional electrons (or holes) provided by these impurity ions. For completeness we have considered all elements in the series even though some of the rutile phases (e.g., FeO_2, CoO_2, and NiO_2) have not been reported, suggesting that *high* concentration rutile-structure alloys of these elements with CrO_2 might not be stable. Our study is, however, aimed at understanding these materials for *low* impurity concentrations and at elucidating trends and qualitative physics.

II. METHODOLOGY

We conducted first-principles-based density function theory (DFT) calculations within the generalized gradient approximation (GGA)[7,8] using the Vienna *Ab initio* Simulation Package (VASP)[9] and projector augmented wave (PAW) pseudopotentials by Kresse and Joubert.[10] We constructed periodic supercells containing 24 atoms, i.e., four tetragonal six-atom rutile cells having metal ions at the corners and body center. The supercell had dimensions $2a \times b \times 2c$ and allowed us to substitute 12.5% of the Cr ions with the chosen impurity ion. All of the eight sites within this supercell are equivalent for adding a single impurity. To check whether the 24 atom supercell was large enough for our purposes, we also calculated the electronic and magnetic structures of Nb and Ru impurities with a 48 atom supercell. The density of states (DOS) changed in expected ways with localized impurity states becoming narrower for the 48 atom cell compared to the 24 atom cell. Since this effect only reinforces our primary

conclusion that impurity states that form within the gap do not destroy the half-metallicity, we tentatively conclude that larger cells do not add sufficient additional information to justify their use in this survey.

In all calculations, we used a $5 \times 9 \times 7$ Monkhorst–Pack[11] k-point grid and a plane wave cutoff of 400 eV. We allowed structural relaxation of the supercell but did not allow for the possibility of complicated extended defects in the rutile structure, which might include deviations from oxygen stoichiometry. In all of our supercells, the number of O anions was twice the number of cations.

At the suggestion of reviewers, we considered the possibility that the substituted cation might prefer an "interstitial" site, i.e., some site other than the one vacated by the Cr ion that was removed from the cell. We concluded that this is unlikely based on the following considerations: Je and Sinnott investigated Frenkel and Schottky defects in TiO_2[12] and found that Schottky defects were unstable by energies ranging from 3.5 to 5.5 eV depending on the model while Frenkel defects were unstable by 2 to 4 eV. The lowest energy Frenkel defect consisted of a displacement of one of the Ti ions to a position at the center of an a–c face of the standard tetragonal rutile cell.

We investigated a Ru ion as a Frenkel defect in a 48 atom CrO_2 supercell, displacing the Ru ion to the center of an a–c face of the standard tetragonal cell corresponding to the lowest energy defect found in Ref. 12. After structural relaxation, which left the basic structure of the cell intact with a vacancy at the position from which the Cr ion was removed, the energy was compared to the energy of the relaxed structure with the Ru ion at the position originally occupied by the Cr ion. The Frenkel defect configuration was 4.4 eV higher in energy.

The initial parameters of the cells used for the substitutional impurity studies were based on the known bulk CrO_2 values ($a = b = 0.4593$ nm, $c = 0.2959$ nm). Each system was relaxed so that the interatomic forces were less than 0.1 eV/Å, before the electronic structure and magnetic moments were calculated.

Plane-wave-based DFT codes generate charge and magnetization densities that extend throughout the computational cell. Any method of assigning a charge or magnetic moment to a particular ion is, to some extent, arbitrary. The total change in the spin-magnetic moment on substituting an impurity atom for a Cr atom is, however, well and unambiguously defined. In these particular systems, moreover, we find that the minority Fermi energy continues to lie in a gap in the DOS even after the substitution. This implies that the number of minority electrons in the cell is an integer. Since the total number of electrons in the cell is also an integer, it follows that the number of majority electrons is an integer and finally that the total spin moment of the cell after the substitution is an integer. Thus, if we assign a moment of 2 μ_B to each of the Cr ions, we can associate the difference between the total cell moment after substitution and 2 $n\mu_B$ with the impurity moment. Here n is the number of Cr ions in the cell after the substitution ($n = 7$ for the calculations based on the 24 atom cell reported here). When we report magnetic moments for individual ions, they are calculated within a sphere of radius 0.9 Å for the 3d ions and 1.0 Å for the 4d ions. We find that the orbital moment is less than 0.05 μ_B for both the Cr and impurity ions, and we neglect its contribution in the following.

III. RESULTS

A. Electronic structure of CrO_2

It is helpful to briefly review the DFT-GGA electronic structure of CrO_2, which we used as a starting point for understanding the effect of placing impurities into this host. The DOS is shown in Fig. 1, where the O-p states and Cr-d states are labeled. The assignment of states to O or Cr ions is, of course, approximate since all of the states are hybridized and the charge and magnetization densities from a DFT calculation cannot be assigned unambiguously to a particular ion. The number of states per atom or a given orbital type, however, is largely conserved by the hybridization so that it is possible to describe the electronic structure in a manner that is consistent with a chemical picture.

In this picture, the oxygen p-states are filled by each oxygen ion, acquiring two additional electrons from the Cr ions. Since there are twice as many O ions as Cr ions, the O ions will be in the (nominal) -2 valence state, and the Cr ions will be in the (nominal) $+4$ valence state. Each Cr ion is surrounded by six O ions, which form a distorted octahedron. The approximate cubic crystal symmetry of the distorted octahedron breaks up the five Cr d states per spin into a lower energy group of three per Cr ion that would be labeled "t_{2g}" if the symmetry were exactly cubic and a corresponding higher energy group of two "e_g" states per Cr ion. This is most easily seen for the minority Cr-d DOS, where the DOS vanishes at an energy that separates a "lump" of DOS that contains three electrons from one that contains two electrons. For the majority channel, the strong exchange interactions push the majority t_{2g} states down in energy so that they overlap slightly with the majority O-p states. In a tight-binding model, this overlap between the O-p and Cr-d majority states requires some degree of direct Cr-d to Cr-d interaction. This is possible in the rutile structure because of the relatively small Cr-Cr distance along the c axis (equal to the c-axis lattice parameter).

The DFT-GGA DOS for nonmagnetic CrO_2 is very similar to the magnetic version with the exception that the majority d states are higher (identical to the minority) and well separated from the O-p states. The Fermi energy falls such that one majority and one minority Cr-d state are occupied. Thus in DFT, the system reduces its energy by generating spin

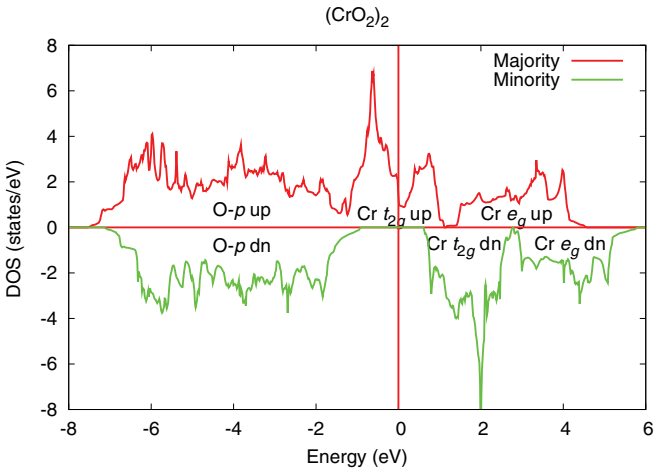

FIG. 1. (Color online) Electronic DOS of CrO_2.

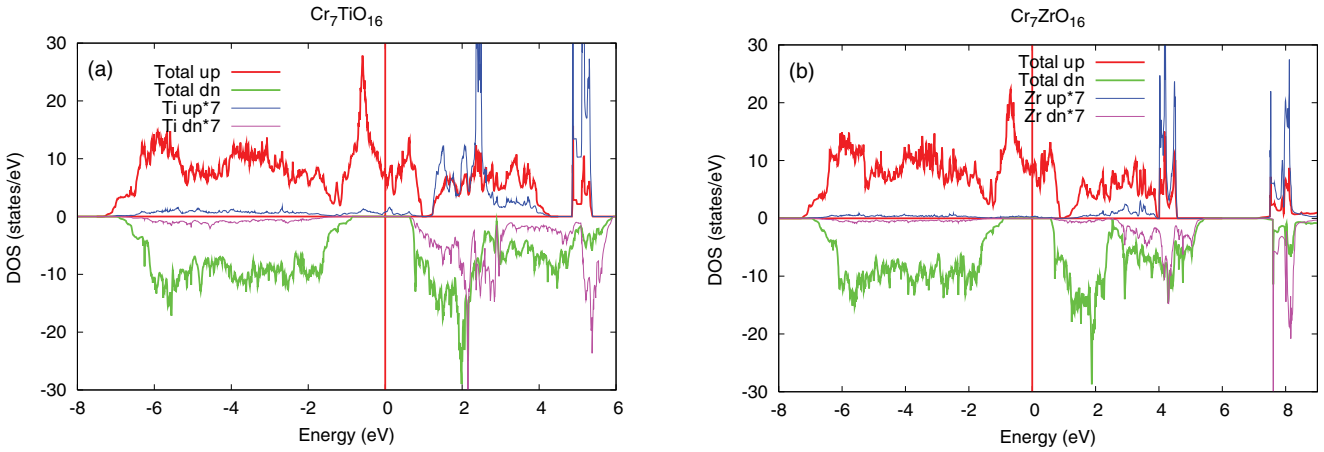

FIG. 2. (Color online) Calculated DOS for (a) Ti and (b) Zr impurities in CrO_2. The total DOS in the 24 atom supercell is indicated by thick lines. The DOS for the Ti and Zr impurities is indicated by thinner lines. The impurity DOS has been multiplied by seven to enhance visibility. The impurity DOS is calculated within a sphere of radius 0.9 Å.

polarization that allows it to push two occupied Cr-*d* states down in energy and simultaneously push the unoccupied *d* states up. The spin-polarized system gains an additional reduction in energy because the majority Fermi energy falls in a pseudogap that forms within the t_{2g} complex.

B. d^0 Cr(Ti)O_2 and Cr(Zr)O_2

Figure 2 shows the calculated DOS for Ti and Zr impurities in CrO_2. Since both impurity ions are surrounded by six oxygen ions, they are in a $+4$ valence state (d^0 configuration), the net moment on the Ti or Zr site is expected to be 0 so that each substituted Ti or Zr reduces the magnetic moment by 2 μ_B. This is in qualitative agreement with our calculations. The net decrease in spin moment associated with either substitution is exactly 2 μ_B. This is clear from the DOS curves. Because the minority band gap is still present and the Fermi energy falls in it, the spin moment is an integer and, because the number of occupied minority states does not change on substitution (the occupied minority states consist of the O 3-*p* states), all of the change in the number of electrons (-2 per substitution) must be accommodated in the majority channel. The moment within 0.9 Å radius spheres surrounding the Ti or Zr sites is not exactly zero but 0.105 for Ti and 0.03 for Zr.

One major difference between Ti and Zr is in the unoccupied part of the DOS where it can be seen that the Zr impurity *d* states lie much higher in energy than those of Ti and have a larger splitting between the t_{2g} and e_g states. Another difference is that there is stronger hybridization of the Ti-*d* states with the O-*p* states due to their closer proximity in energy.

C. d^1 Cr(V)O_2 and Cr(Nb)O_2

Figure 3 shows the calculated DOS for V and Nb impurities in CrO_2. Both of these impurity atoms have five valence electrons, one less than the Cr atom that they replace, so that when they are ionized by the quasioctahedral oxygen environment, their configuration is expected to become d^1. We find that the total spin moment of the cell after the substitution is reduced from 16 to 15, indicating that the "V moment" and the "Nb moment" have aligned ferromagnetically with the magnetization of the host. The use of quotes in the preceding sentence is intended to indicate that the common

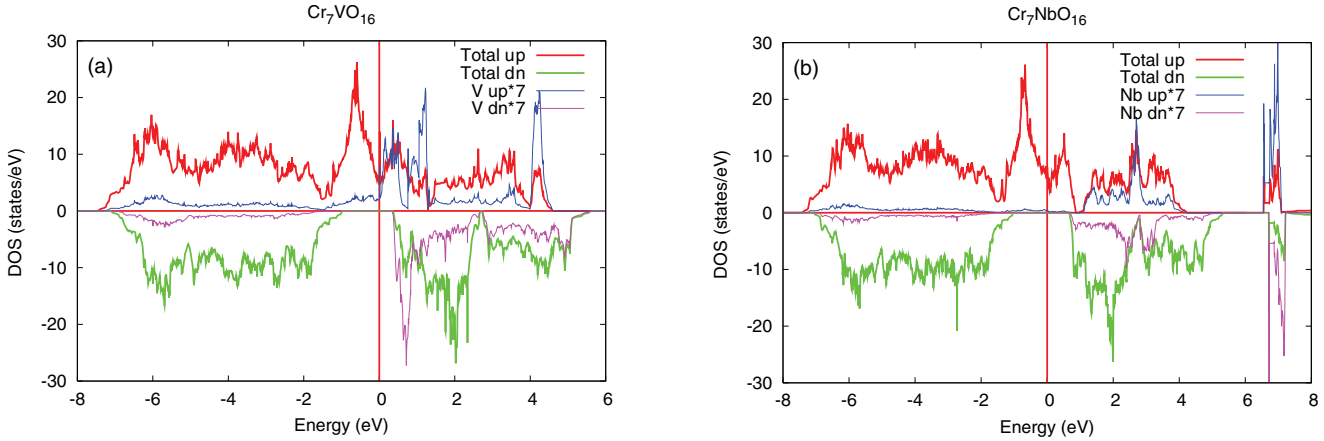

FIG. 3. (Color online) Calculated DOS for (a) V and (b) Nb impurities in CrO_2. The total DOS in the 24 atom supercell is indicated by thick lines. The DOS for the V and Nb impurities is indicated by thinner lines and has been multiplied by seven. The impurity DOS is evaluated within a sphere of radius 0.9 Å centered on the impurity site.

TABLE I. Summary of magnetic moment values for 3*d* substitution of CrO_2. Up (down) implies ferromagnetic (antiferromagnetic) alignment with host Cr. The magnetic moment units are μ_B.

Element	Ti	V	Cr	Mn	Fe	Co	Ni	Cu
Nominal spin configuration of Impurity	0 up 0 down	1 up 0 down	2 up 0 down	3 up/0 dn or 0 up/ 3 dn	1 up 3 down	2 up 3 down	2 up 4 down	2 up 5 down
Total cell moment (μ_B)	14	15	16	17 or 11	12	13	12	11
Impurity moment (μ_B)	0.10	0.46	n/a	2.52 FM - 2.17 AF	−1.27	−0.17	−0.52	−0.60
Average Cr moment (μ_B)	1.79	1.85	1.80	1.80 FM 1.76 AF	1.77	1.73	1.66	1.59
Average O moment (μ_B)	0.00	0.00	0.01	0.02 FM				
−0.01 AF	−0.02	−0.02	−0.03	−0.04				
Average moment of O nearest impurity (μ_B)	0.02	0.02	n/a	0.05 FM 0.03 AF	−0.04	−0.04	−0.05	−0.09
Distance to apical O (Å)	1.97	1.93	1.91	1.90	1.89	1.89	1.99	2.02
Distance to planar O (Å)	1.96	1.88	1.91	1.90	1.88	1.90	1.89	2.01

notion of the spin moment "on" a transition metal ion may be an oversimplification, at least within this type of mean field calculation. For CrO_2, the moment within a 0.9 Å radius Cr sphere is 1.796 or 90% of the total moment per Cr ion (with nominal spin 2 μ_B). For the V impurity, the sphere moment is 0.455 μ_B or 45.5% of its nominal spin, and for Nb it is only 0.069 μ_B or less than 7%.

We can obtain a qualitative understanding of the apparent missing magnetic moment from the information listed in Tables I and II. For the cell with the Nb substitution, the average spin moment within the six O ion spheres (radius 1.45Å) increases from 0.0105 μ_B to 0.0465 μ_B. This would account for 0.22 μ_B. The average moment within the seven Cr spheres increases from 1.796 μ_B to 1.883 μ_B. This is sufficient to account for 0.61 μ_B. It should be noted that the sum of the sphere moments will not, in general, equal the total cell moment, but it is clear that the magnetization associated with the Nb substitution is quite diffuse.

The situation is similar for the V impurity, if less dramatic. In addition to the 0.455 μ_B within the V sphere, the average

TABLE II. Summary of magnetic moment values for 4*d* substitution of CrO_2. Up (down) implies ferromagnetic (antiferromagnetic) alignment with host Cr. The magnetic moment units are μ_B.

Element	Zr	Nb	Mo	Tc	Ru	Rh	Pd	Ag
Nominal spin configuration of Impurity	0 up 0 down	1 up 0 down	2 up 0 down	3 up 0 down	1 up 3 down	2 up 3 down	3 up 3 down	2 up 5 down
Total cell moment (μ_B)	14	15	16	17	12	13	14	11
Impurity moment (μ_B)	0.03	0.07	0.27	1.08	−0.93	−0.21	0.13	−0.36
Average Cr moment (μ_B)	1.79	1.88	1.94	1.90	1.77	1.75	1.77	1.56
Average O moment (μ_B)	−0.01	0.02	0.02	0.02	−0.04	−0.03	−0.00	−0.05
Average moment of O nearest impurity (μ_B)	0.03	0.05	0.04	0.08	−0.07	−0.04	−0.02	−0.09
Distance to apical O (Å)	2.09	2.01	1.96	1.95	1.97	1.98	2.00	2.15
Distance to planar O (Å)	2.09	1.9	1.94	1.96	1.98	2.00	2.02	2.16

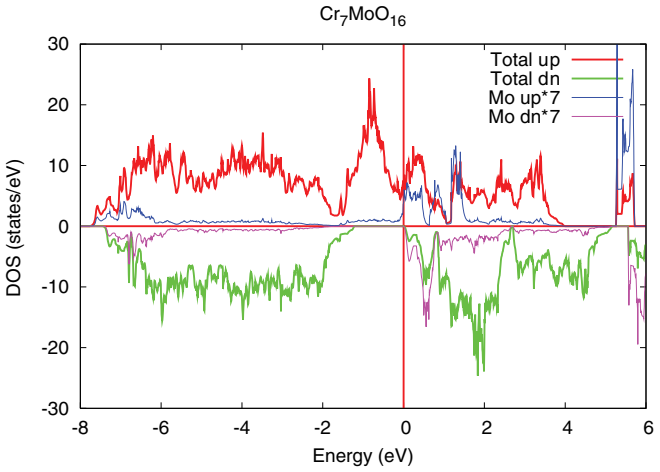

FIG. 4. (Color online) Calculated DOS for Mo impurity in CrO_2. The total DOS in the 24 atom supercell is indicated by thick lines. The DOS for the Mo impurity site is indicated by thinner lines and has been multiplied by seven. The impurity DOS is evaluated within a sphere of radius 0.9 Å centered on the impurity site.

moment of the six neighboring O ions increases from 0.0105 to 0.0127, accounting for 0.013 μ_B. The moment within the seven Cr spheres increases from 1.796 μ_B to 1.851 μ_B, accounting for 0.385 μ_B.

D. d^2 Cr(Mo)O_2

Figure 4 shows the calculated DOS for a Mo impurity in CrO_2. Mo is iso-electronic with Cr. Both atoms have six valence electrons. Their ions in the octahedral O environment are expected to be in the d^2 state. The calculated magnetic moment of 16 μ_B for the Cr_7MoO_{16} supercell is consistent with this state picture. However, from Fig. 4 it appears that Mo is in something closer to a d^0 state since less than 12.5% of the expected 2 μ_B is within the 0.9 Å radius sphere. This picture is also supported by the increased moment on the O ions surrounding the Mo impurity and by the enhancement of the moments within the Cr ion spheres, as shown in Tables I and II.

From Fig. 4, it is also clear that the shift of the impurity 4*d* states to higher energy compared to 3*d* is reduced in Mo compared to Nb. The Mo minority impurity t_{2g} states lie just above the Fermi energy so that the system is only barely a half-metal. There is a large splitting between the t_{2g} and e_g impurity states.

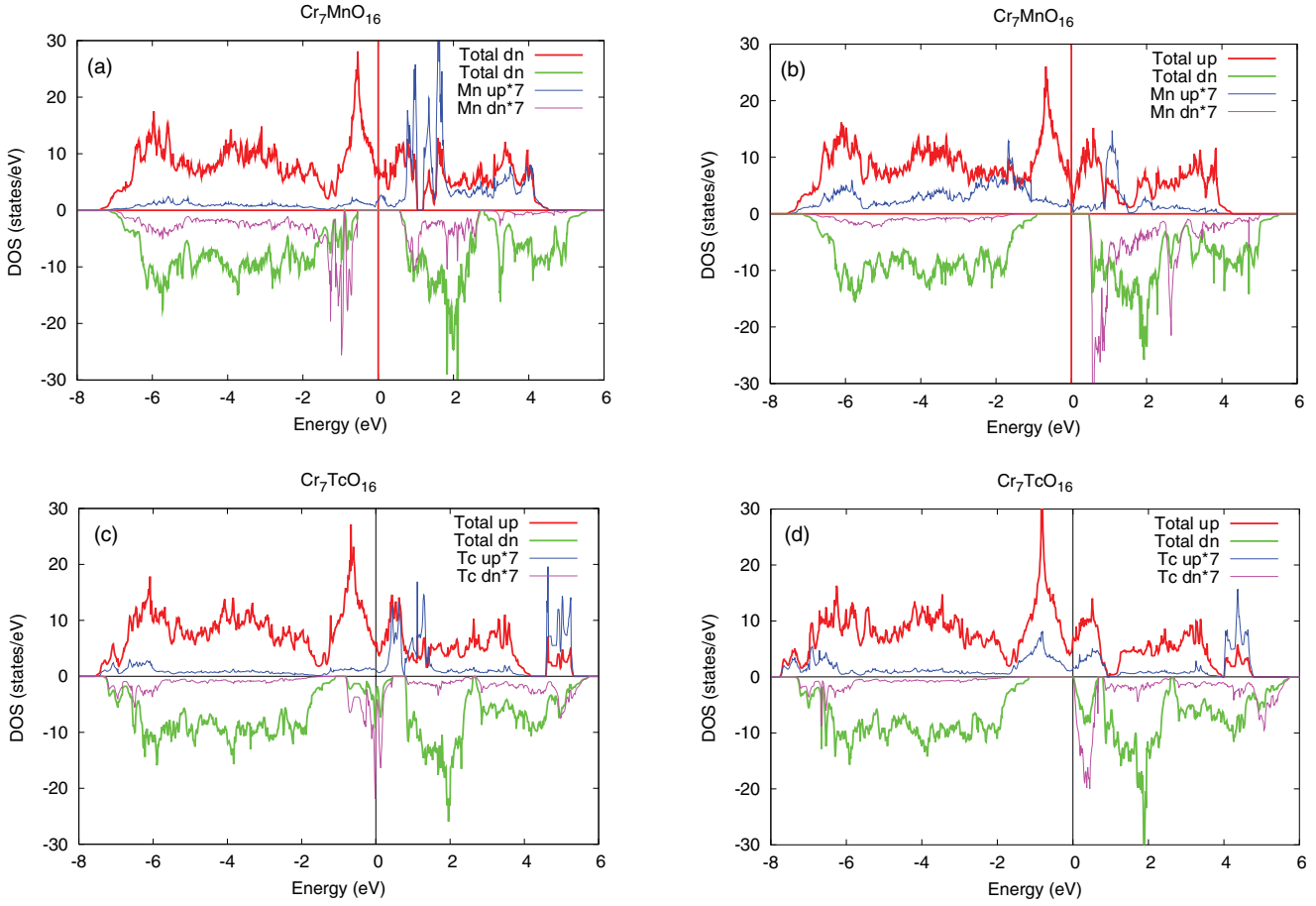

FIG. 5. (Color online) Calculated DOS for Mn and Tc impurities in CrO_2. (a) Solution to DFT-GGA equations for Mn impurity with total moment per cell of 11 μ_B and (b) 17μ_B. (c) Solution to DFT-GGA equations for Tc impurity with total moment per cell of (c) 13.5 μ_B and (d) 17 μ_B. The total DOS in the 24 atom supercell is indicated by thick lines. The DOS for the Mn impurity site is indicated by thinner lines and has been multiplied by 7. The impurity DOS is evaluated within a sphere of radius 0.9 Å centered on the impurity site.

E. d^3 Cr(Mn)O_2 and Cr(Tc)O_2

Figure 5 shows the calculated DOS for a Mn impurity [(a) and (b)] and for a Tc impurity [(c) and (d)] in our 24 atom supercell. For all substitutions, we searched for both FM (impurity moment aligned with host moments) and AFM (impurity moment antialigned with host moments) solutions to the DFT-GGA equations. For the impurities presented in Figs. 1–4, we were only able to obtain one solution for each impurity. For Mn and Tc impurities, however, we were able to obtain multiple solutions. For Mn, the two quite different solutions appear to be nearly degenerate in energy. One solution (panel a) generates a low moment. For this case, we find a total cell moment of 11 μ_B, i.e., a net decrease of 5 μ_B on substitution of a Cr atom by a Mn atom. Since a Mn^{4+} ion is expected to be in the d^3 state, we would naturally associate the decrease of 5 μ_B with a Mn ion having a moment of $3\mu_B$ aligned antiferromagnetically. This is qualitatively what our calculation describes. The moment within the 0.9 Å radius sphere is -2.17 μ_B rather than -3, but, as we have emphasized, the sphere radius is somewhat arbitrary. Part of the difference is no doubt related to the strong hybridization of the minority Mn-d states with the O-p states that can be seen in Fig. 5). This picture is supported by the calculated moments within the O-ion spheres (radius = 1.45 Å), which average -0.026 μ_B on the six O ions surrounding the Mn ion compared to $+0.0105$ μ_B for the O spheres in CrO_2. It is remarkable that if the two Mn impurity solutions are indeed within 3 meV in energy with the AFM phase lower in energy as we have calculated, it should be (barely) possible to effect a transition with a 9 T laboratory magnet.

The other solution that we found [Fig. 5(b)] gave a total cell moment of 17 μ_B and was calculated to be approximately 3 meV higher in energy than the 11 μ_B solution. The natural interpretation would be that in this case, the Mn d^3 ion with a spin moment of 3 μ_B is aligned ferromagnetically with the host-spin moments. This picture is consistent with the calculated moment within the (0.9 Å radius) sphere of 2.52 μ_B. Experimental observation of a marked decrease in magnetization with Mn substitution[13] supports our picture of a large negative moment on the Mn ion.

We also found two solutions for the Tc impurity. When the DFT-GGA equations are solved using VASP and following normal procedures beginning with a local impurity moment that is either aligned or antialigned, one obtains a solution with a moment of approximately 13.5 μ_B. For this solution [Fig. 5(c)], the impurity t_{2g} states sit astride the Fermi energy and are approximately half-filled. We searched for additional states with 11 or 17 μ_B per cell corresponding to AFM or FM alignment of the impurity moment using a feature of VASP that allows one to constrain the total cell moment. Solutions with 11 μ_B were not stable when the constraint was removed, but solutions with 17 μ_B were stable [Fig. 5(d)] and were lower in energy than the 13.5 μ_B solution [Fig. 5(c)] by 173 meV.

F. d^4 Cr(Fe)O_2 and Cr(Ru)O_2

Figure 6 shows the DOS for (a) an Fe impurity and (b) a Ru impurity in CrO_2. Fe and Ru each have eight valence electrons so their $4+$ ions will have four electrons. The net change in moment due to the substitution is -4 μ_B in both cases. From the DOS it is clear that this is accomplished by the three minority t_{2g} states moving below the Fermi energy. For Fe, the impurity minority t_{2g} states are moved down to the top of the O-p states so that the band gap is not greatly reduced from that of CrO_2. For Ru, on the other hand, the occupied minority t_{2g} states are in the gap and significantly reduce it.

G. d^5 Cr(Co)O_2 and Cr(Rh)O_2

Figure 7 shows the DOS for Co and Rh impurities in CrO_2. Co and Rh would have a d^5 configuration as $4+$ ions. Similar to Fe and Ru, for Co and Rh, the minority t_{2g} states are occupied. In both cases they are shifted down to the top of the minority O-p bands so that sizable minority band gaps survive the substitution.

H. d^6 Cr(Ni)O_2 and Cr(Pd)O_2

Figure 8 shows the calculated DOS for Ni and Pd impurities in CrO_2. Ni and Pd impurities are expected to be in the d^6 configuration. If they follow the rule of filling the three minority t_{2g} states, these ions would contribute no magnetization to the

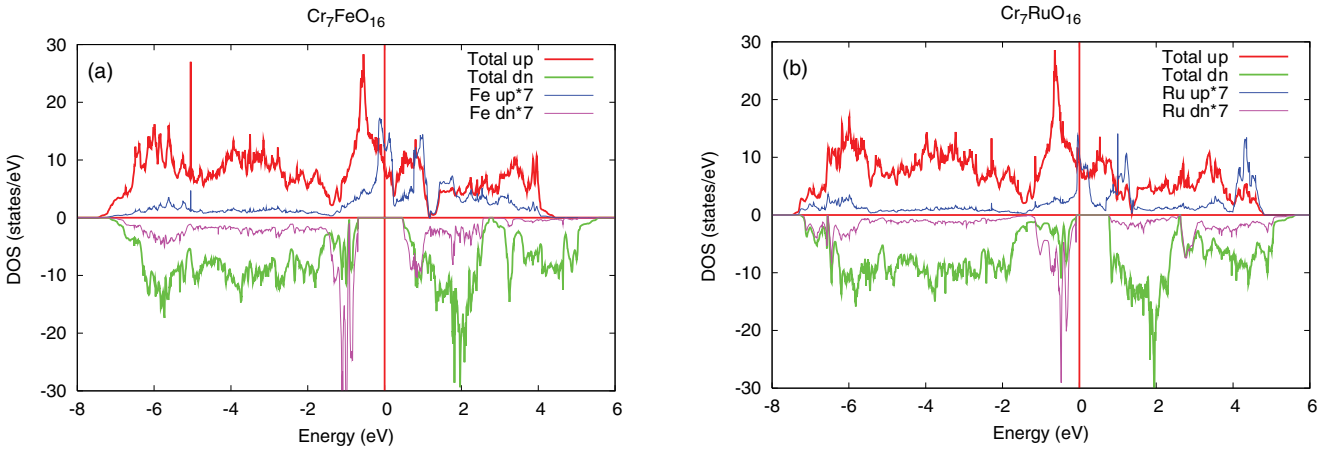

FIG. 6. (Color online) Calculated DOS for (a) Fe and and (b) Ru impurities in CrO_2. The total DOS in the 24 atom supercell is indicated by thick lines. The DOS for the Fe and Ru impurities is indicated by thinner lines and has been multiplied by seven. The impurity DOS is evaluated within a sphere of radius 0.9 Å centered on the impurity site.

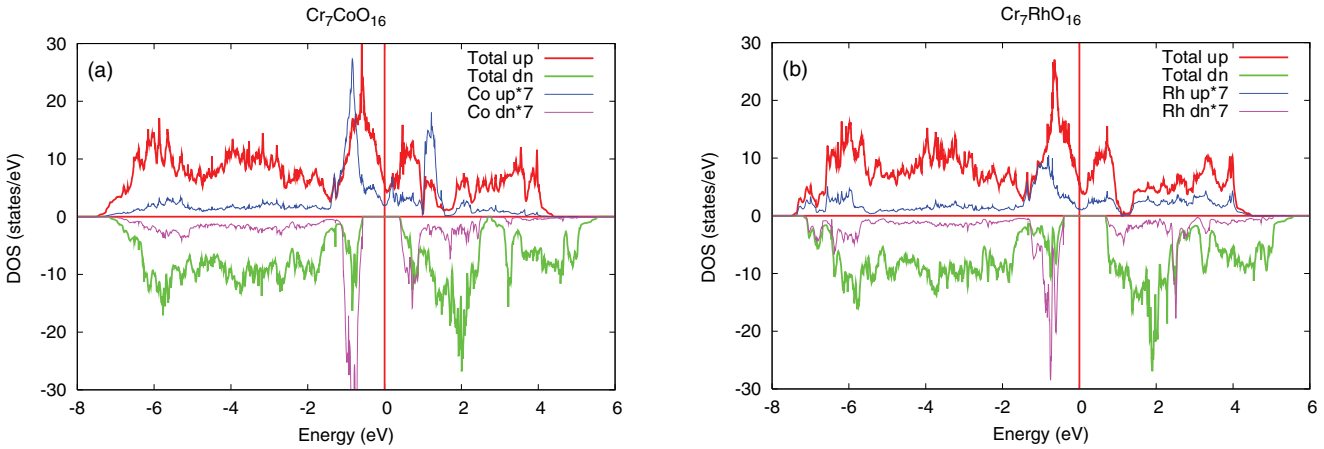

FIG. 7. (Color online) Calculated DOS for (a) Co and and (b) Rh impurities in CrO_2. The total DOS in the 24 atom supercell is indicated by thick lines. The DOS for the CO and Rh impurities is indicated by thinner lines and has been multiplied by seven. The impurity DOS is evaluated within a sphere of radius 0.9 Å centered on the impurity site.

cell so that the total moment would decrease by 2 μ_B per impurity. That is what happens for the Pd impurity. The three minority t_{2g} states are filled, and the two minority e_g states are empty. The three minority states induced by the impurity must be compensated by the remaining three electrons contributed by the Pd ion so that the total moment induced by the impurity is simply $-2\ \mu_B$, i.e., the moment that would have been contributed by the replaced Cr ion. For Ni, the case is somewhat different. The e_g levels are split, with one e_g level being filled and the other empty. This leads to four minority electrons per impurity and two majority, so that the total moment induced by the impurity is $-3\ \mu_B$.

Consider adding an additional electron to the DOS of Fig. 7. One way that it can be done is exemplified by Pd, which simply adds it to the majority, pulling the majority states down slightly relative to the minority to accommodate the additional electron. The system with a Ni impurity adds the electron in a different way by distorting the octahedron so that the cation to apical O distances are increased from 1.91 Å to 1.99 Å. This causes the two e_g states to split. The system can then occupy the lower one and reduce its energy. This "strategy" works much better for Ni than for Pd because the Ni impurity e_g states have moved into the gap, which makes them very narrow. It can be shown that because they are in the gap, they would be delta-functions if there were only interactions between the Cr ions and their surrounding O ions. In fact, there is significant direct interaction between neighboring Cr ions in the direction of the c axis. One of the e_g orbitals, however, is oriented orthogonal to this direction so it is extremely narrow. The splitting of the e_g states in the CrO_2 gap is an example of a Jahn–Teller distortion.[14]

I. d^7 Cr(Cu)O_2 and Cr(Ag)O_2

The DOS for Cu and Ag impurities in CrO_2 is shown in Fig. 9. Cu and Ag are expected to be in the d^7 configuration as impurities in CrO_2. From Fig. 9, it is clear that they prefer to have all of their minority d states occupied. In both cases the minority impurity t_{2g} states hybridize strongly with the O-p states. The minority e_g states remain in the gap and occupy a very narrow energy range. Since five of the seven electrons of the d^7 ions go into the minority, the net change

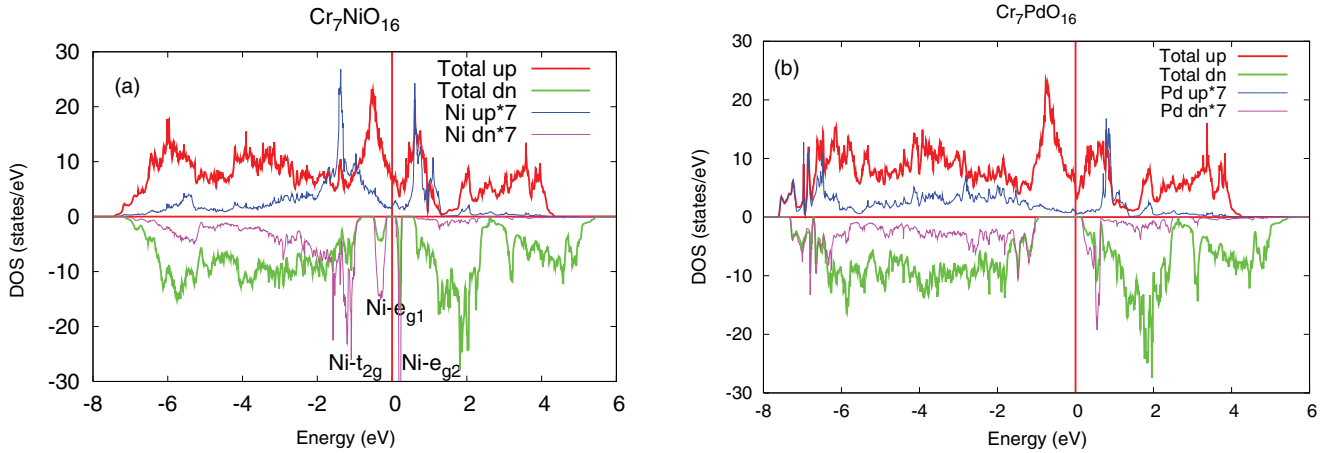

FIG. 8. (Color online) Calculated DOS for (a) Ni and and (b) Pd impurities in CrO_2. The total DOS in the 24 atom supercell is indicated by thick lines. The DOS for the Ni and Pd impurities is indicated by thinner lines and has been multiplied by seven. The impurity DOS is evaluated within a sphere of radius 0.9 Å centered on the impurity site.

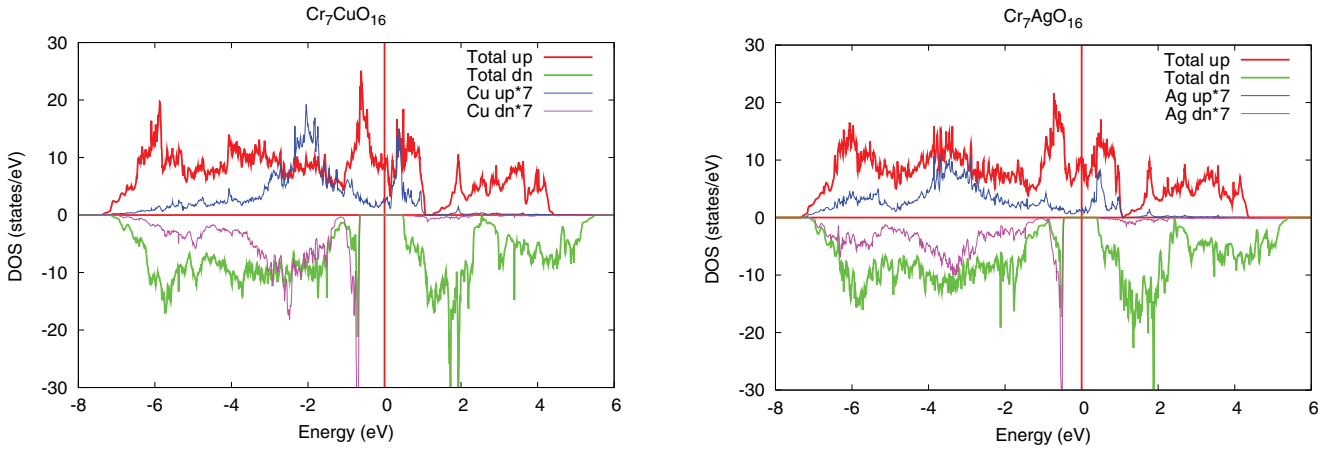

FIG. 9. (Color online) Calculated DOS for (a) Cu and (b) Ag impurities in CrO_2. The total DOS in the 24 atom supercell is indicated by thick lines. The DOS for the Cu and Ag impurities is indicated by thinner lines and has been multiplied by seven. The impurity DOS is evaluated within a sphere of radius 0.9 Å centered on the impurity site.

in magnetization induced by a Cu or Ag substitution is -5 μ_B, consisting of the loss of the two majority electrons on the Cr ion and the net three minority electrons on the Cu or Ag ions.

IV. MOMENT RULE

Within DFT-GGA, the following rule appears to govern the ground-state magnetic moment for 3*d* and 4*d* transition metal impurities in CrO_2. The number of minority electrons added by the impurity increases from zero (Ti, Zr, V, Nb, Cr, Mo, Mn, Tc) to three (Mn, Fe, Ru, Co, Rh, Ni*, Pd) to five (Cu, Ag) as one proceeds across the 3*d* and 4*d* transition metal series. Mn is listed twice since the states with zero and three minority electrons added seem to be close in energy. Ni has an asterisk because it is an exception to the zero-three-five rule. The origin of this rule is almost certainly the grouping of states caused by the approximate cubic field of the oxygen ion distorted octahedron into a group of three and a group of two at higher energy coupled with the sharpness of these states as they cross the rather large gap in the minority DOS of CrO_2. Ni is the exception since its ground state is accompanied by an exceptionally large distortion of the oxygen octahedron that causes a relatively large splitting of the two e_g states.

From the calculated DOS, the three t_{2g} and two e_g states are each spread over an energy range that varies from system to system but is typically $2-3$ eV. Nevertheless, the calculated change in spin moment upon substitution is consistent with a picture in which these states have no dispersion. Thus the number of occupied minority *d* states on the impurity is 0 (d^0–d^3 impurities) then jumps to three as all of the t_{2g} minority impurity states (d^3–d^6 impurities) are occupied and finally jumps to five as the two e_g minority impurity states are filled (d^7 impurities). Part of the reason for this behavior is that the dispersion of the minority impurity states may be significantly decreased if they fall in the minority gap of the CrO_2 where there are no *d* states with which to interact. This result, at least for this system, helps to reconcile the band and crystal field pictures of transition metal oxides.

V. DELOCALIZED MOMENTS

Despite the fact that the moment rule discussed in the last section appears to be consistent with a picture of

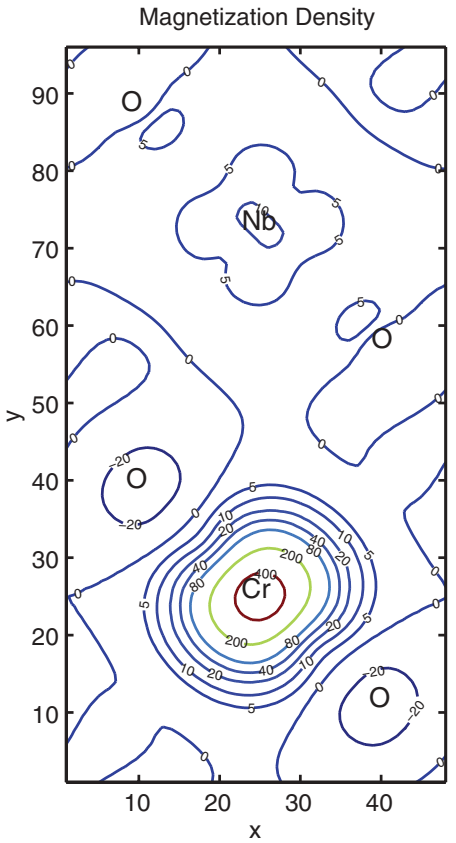

FIG. 10. (Color online) Magnetization as a function of *x* and *y* for fixed *z*. *z* is parallel to the *c* axis of the tetragonal cell. There is very little magnetization in the vicinity of the Nb ion, but enhanced magnetization on its neighboring O ions compared to O atoms bonded to Cr ions, which have a negative magnetization density. The *x* and *y* axes of the cell are discretized into 48 and 96 units, respectively. Each unit corresponds to 0.0094 nm.

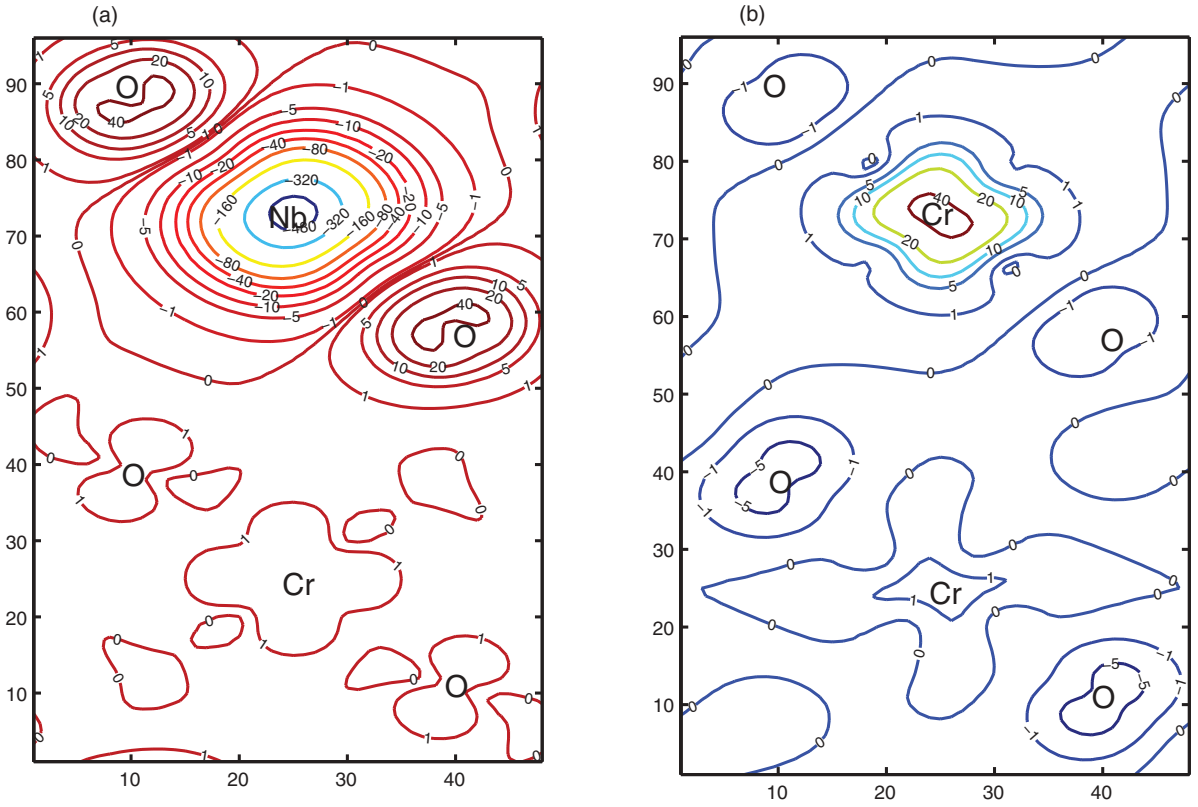

FIG. 11. (Color online) Difference in magnetization density between Cr_8O_{16} and Cr_7NbO_{16} for two cuts through the supercell for fixed z. (a) The panel shows the same cut as in Fig. 10. The elimination of the magnetization on the Nb site (difference is negative) and its enhancement on neighboring O ions can be seen. (b) The panel shows the difference in magnetization for a cut through a plane parallel to that of the left panel that does not contain a Nb substitution showing enhancement of the magnetization on the Cr ions immediately above and below the Nb ion (along the c axis) is enhanced. The x (short) and y (long) axes are discretized into 48 and 96 units, respectively. Each unit is 0.0094 nm.

localized, dispersionless minority electrons within GGA-DFT, this picture seems to be significantly distorted for the majority electrons, especially for some of the 4*d* impurities. In this section, we investigate the curious result mentioned in our discussion of Table II that although the moment associated with a Nb impurity is 1 μ_B, as expected for a d^1 Nb^{4+} ion, this moment does not appear to reside on the Nb ion. Table II indicates that less than 7% of the moment associated with the impurity resides within a sphere of radius 0.9 Å centered at the Nb ion. Figure 10 is a contour plot of the magnetization density for a slice through the cell parallel to an (001) plane. This slice cuts through the positions of a Cr ion and a Nb ion. It can be seen that the magnetization density almost vanishes in the region surrounding the Nb ion. It can also be seen that the magnetization near the O ions neighboring the Nb ion is increased compared to those adjacent to a Cr ion. In fact, the increase in the magnetization in the vicinity of the neighboring O ions exceeds the magnetization in the vicinity of the Nb ion.

Figure 11 shows the calculated difference between the magnetization for cells of composition Cr_7NbO_{16} and Cr_8O_{16}. In order to perform the subtraction, the magnetization density for Cr_8O_{16} was calculated for the same coordinates used for Cr_7NbO_{16}, i.e., the relaxed cell as distorted by the impurity.

A similar effect can be seen for the magnetization of a Mo impurity in CrO_2. Although Mo is isoelectronic with Cr and the calculated magnetic moment is unchanged when Mo is substituted for Cr, the calculated magnetization density is quite small in the vicinity of the Mo ion, and the magnetization is enhanced on the Cr ions, especially the ones directly above and below the Mo along the c axis.

VI. RELEVANCE OF CORRELATION EFFECTS

In addition to the DFT-GGA calculations, we performed exploratory calculations using GGA + U with $U = 3.0$ eV and $J = 0.9$eV on both the Cr and impurity ions for the Nb (minority d^0), Ru (minority d^3), and Ni (minority d^4) impurities. As expected, the occupied states were moved down relative to unoccupied states. The Jahn–Teller splitting of the Ni e_g states is enhanced, and our general picture of transition-metal-doped CrO_2 remaining a half-metal with the moment rule, as described previously, is reinforced. We have not conducted a full GGA + U investigation due to the difficulty in obtaining accurate U and J parameters and because GGA + U does not qualitatively change the picture presented by the parameterless GGA calculations.

VII. CONCLUSIONS

We calculated the electronic structure of CrO_2 with 3*d* and 4*d* transition metal ions as impurities. All of the considered systems were relaxed structurally. From our calculations, it can

be seen that rutile CrO_2 remains a half-metal when impurity elements are substituted for Cr forming $Cr_{0.875}Z_{0.125}O_2$. We find that the net change in spin magnetic moment can be understood in terms of a picture in which zero (d^0–d^3 impurities), three (d^3–d^6 impurities), or five (d^7 impurities) electrons from the impurity occupy the minority spin channel. This causes the net impurity moment to align antiferromagnetically with the Cr moments when the impurity has more than three valence electrons (the FM and AFM configurations are nearly degenerate in Mn).

We find a surprising result for the 4*d* substitutions Nb and Mo, which yield a total moment consistent with the notion that Nb has a moment of 1 μ_B and Mo a moment of 2 μ_B; yet, a detailed study of the magnetization shows that there is only a very small moment on the Mo ion and even less on the Nb. These substitutions will have a profound effect upon the electronic states at the Fermi energy, which remain fully spin-polarized. These unexpected effects may offer the opportunity to engineer rutile-based heterostructures with modified transport properties and exchange interactions.

ACKNOWLEDGMENTS

The authors greatly appreciated input from Dr. Claudia Mewes of the MINT Center who read the paper and discussed various aspects with us. Some of the calculations were performed on the University of Alabama High-Performance Cluster. We also thank Professors Arunava Gupta and Patrick LeClair for helpful suggestions. This work was supported by the following grants: NSF MRSEC Grant No. 0213985 and NSF Rutiles project Grant No. 0706280, NSF Career Award No. 0952929.

[1] A. Gupta (private communication, 2010).
[2] H. W. Verleur, A. S. Barker, and C. N. Berglund, Phys. Rev. **172**, 788 (1968).
[3] K. Schwarz, J. Phys. F: Met. Phys. **16**, L211 (1986).
[4] V. Eyert, Ann. Phys. **11**, 650 (2002).
[5] K. B. Chetry, H. Sims, W. H. Butler, and A. Gupta, Phys. Rev. B **84**, 054438 (2011).
[6] M. E. Williams, W. H. Butler, C. K. Mewes, H. Sims, M. Chshiev, and S. K. Sarker, J. Appl. Phys. **105**, 07E510 (2009).
[7] J. P. Perdew, in *Electronic Structure of Solids*, edited by P. Ziesche and H. Eschrig (Akademie Verlag, Berlin, 1991), p 11.
[8] J.P. Perdew, K. Burke, and M. Ernzerhof, Phys. Rev. Lett. **77**, 3865 (1996).
[9] G. Kresse and J. Furthmüller, Comput. Mater. Sci. **6**, 15 (1996).
[10] G. Kresse and D. Joubert, Phys. Rev. B **59**, 1758 (1999).
[11] H. J. Monkhorst and J. D. Pack, Phys. Rev. B **13**, 5188 (1976).
[12] J. Je and S. B. Sinnott, J. Am. Ceram. Soc. **88**, 737 (2005).
[13] B. Martínez, J. Fontcuberta, M. J. Martínez-Lopez, and J. A. Alonso, J. Appl. Phys. **87**, 6019 (2000).
[14] H.A. Jahn and E. Teller, Proc. R. Soc. London A **161**, 220 (1937); H. A. Jahn, *ibid.* **164**, 117 (1938).